sustainability

MDPI

Article

Mechanisms Governing the Formation and Long-Term Sustainment of a Northeastward Moving Southwest Vortex

Kang-Quan Yang [1,2], Di-Xiang Xiao [1,2], Xing-Wen Jiang [2,3,*], Zi-Rui Li [4] and Shen-Ming Fu [5,*]

1 Sichuan Meteorological Observatory, Chengdu 610072, China; yangkangquan@aliyun.com (K.-Q.Y.); xiaodx75@163.com (D.-X.X.)
2 Heavy Rain and Drought–Flood Disasters in Plateau and Basin Key Laboratory of Sichuan Province, Chengdu 610072, China
3 Institute of Plateau Meteorology, China Meteorological Administration, Chengdu 610072, China
4 School of Earth Sciences, Yunnan University, Kunming 650091, China; llizirui@126.com
5 International Center for Climate and Environment Sciences, Institute of Atmospheric Physics, Chinese Academy of Sciences, Beijing 100029, China
* Correspondence: xingwen.jiang@yahoo.com (X.-W.J.); fusm@mail.iap.ac.cn (S.-M.F.)

Abstract: From 10 July to 12 July 2021, a long-lived (~66 h) southwest vortex (SWV), moved from Southwest China to Northeast China and caused a series of heavy rainfall events. This SWV case was rarely seen, as its lifespan was much longer than the SWVs' mean lifespan, and the vast majority of SWVs showed a quasi-stationary behavior. It was found that the SWV formed and sustained in favorable background environments, which were characterized by a strong upper-level divergence (related to the South Asia High), a notable middle-tropospheric warm advection (related to a shortwave trough), and a vigorous low-level jet. The SWV showed remarkable interactions with a middle-tropospheric mesoscale vortex. The strong southwesterly wind in the eastern section of a deep shortwave trough east of the Tibetan Plateau acted as the steering flow for the northeastward movement of both vortices. Vorticity budget showed that the convergence-related vertical stretching dominated the SWV's formation and development; the convection-related upward transport of cyclonic vorticity was the most favorable factor for the SWV's sustainment, whereas, during the decaying stage, the SWV dissipated mainly due to the tilting effects and the net export transport of cyclonic vorticity. Backward trajectory analyses showed that most of the air particles that formed the SWV (at its formation time) were sourced from the lower troposphere. These air particles mainly ascended and experienced a rapid increase in cyclonic vorticity during the SWV's formation stage. The topography of the Yunnan–Guizhou Plateau was crucial for the SWV's formation, as around a half of the air particles (that formed the SWV) came from this region. Most of these air particles enhanced in their cyclonic vorticity and convergence when they descended along the topography of the plateau.

Keywords: mesoscale vortex; southwest vortex; heavy rainfall; vorticity budget

check for updates

Citation: Yang, K.-Q.; Xiao, D.-X.; Jiang, X.-W.; Li, Z.-R.; Fu, S.-M. Mechanisms Governing the Formation and Long-Term Sustainment of a Northeastward Moving Southwest Vortex. *Sustainability* **2023**, *15*, 9255. https://doi.org/10.3390/su15129255

Academic Editor: Mohammad Aslam Khan Khalil

Received: 7 May 2023
Revised: 29 May 2023
Accepted: 6 June 2023
Published: 8 June 2023

1. Introduction

Over Southwest China, there is a unique type of mesoscale vortex [1–3], which is named as the southwest vortex (SWV). The SWVs are mainly generated in the regions around the Sichuan Basin east of the Tibetan Plateau [4–14], and they frequently induce heavy rainfall that cause severe flooding events. For example, in mid July 1981, affected by a strongly developed SWV, a once-in-a-century catastrophic flood occurred in Sichuan [4]; from 28 to 30 July 1993, a series of SWV-related strong rainstorms occurred in the south-western section of the Sichuan Basin, during which the 24 h precipitation in Emeishan City reached up to 509.5 mm, breaking the 40-year record of extreme daily precipitation in Sichuan [14,15]; in the 2020 abnormal Mei-Yu season, the Sichuan Basin experienced a series of flooding events, most of which were caused by southwest vortices [13].

Due to its great importance, tremendous efforts have been made to further the understanding of the SWVs, as this is critical for improving the forecasts of SWVs-related heavy precipitation. For instance, Chen and Min [6], He et al. [14], Fu et al. [10], and Feng et al. [9] conducted statistical studies on the SWVs and they found that the SWVs were mainly located in the lower troposphere, and most of them could not move out from the Sichuan Basin. Luo [16] and Wang and Tan [17] confirmed the crucial role of the effects from the topography on the formation and development of the SWVs. Ni et al. [18] analyzed a SWV that caused a severe flooding event in Sichuan and Chongqing. They pointed out that heavy precipitation appeared in the vortex's development phase, and, after the vortex's dissipation, the cloud water content increased significantly. Cheng et al. [5] studied a composite precipitation event and proposed that the interaction between the Tibetan Plateau vortex and the SWV could enhance the rainfall notably. Chen et al. [8] investigated the interactions between SWVs and mesoscale convective systems (MCSs), and they found that the heaviest rainfall tended to appear in the coupling stage of the SWVs and MCSs.

According to previous studies [9,10], different types of SWVs showed notably different features. This indicated that more analyses of SWVs are needed to reach a more comprehensive understanding of this type of vortex. From 10 July to 12 July 2021, a SWV formed in the northern section of the Sichuan Basin. After formation, the vortex moved northeastward and caused a series of heavy rainfall events along its track (Figure 1). This event deserved a detailed study, as (i) the mean lifespan of a SWV was around 27.5 h [10], whereas the SWV in the present study lasted for a lifespan of ~66 h, and (ii) most of the SWVs could not vacate the Sichuan Basin [9,10], whereas the SWV case in this study moved northeastward to the location as far as the northern section of Hebei Province (Figure 1a). Therefore, the primary scientific purpose of this study is to show the mechanisms governing the formation and long-term sustainment of the SWV, and, also, we discuss the favorable conditions for the vacating and northeastward moving of the vortex. The reminder of this paper includes: Section 2 shows the data and methods used in this study; Section 3 presents the overview of the rainfall event; Section 4 discusses the detailed evolution of the SWV; Section 5 investigates the evolutionary mechanisms of the SWV; and, finally, a conclusion and a discussion are reached in Section 6.

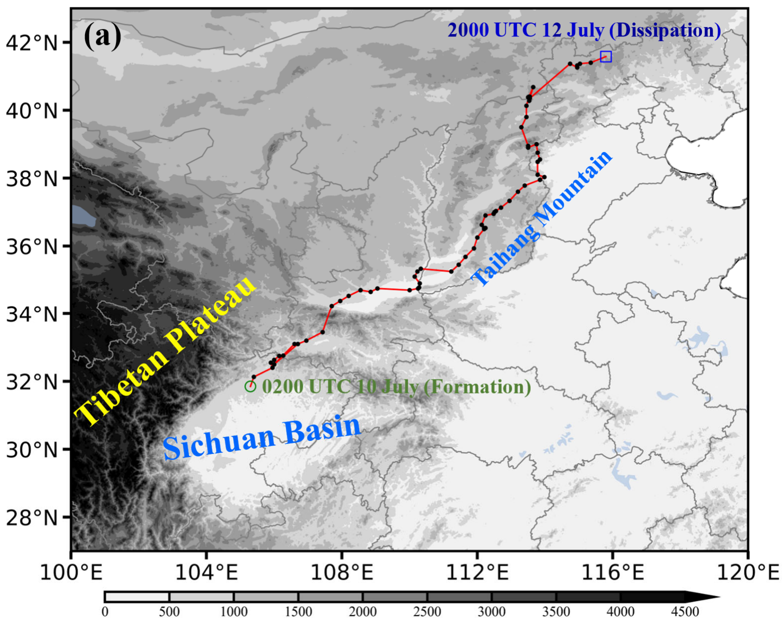

Figure 1. *Cont.*

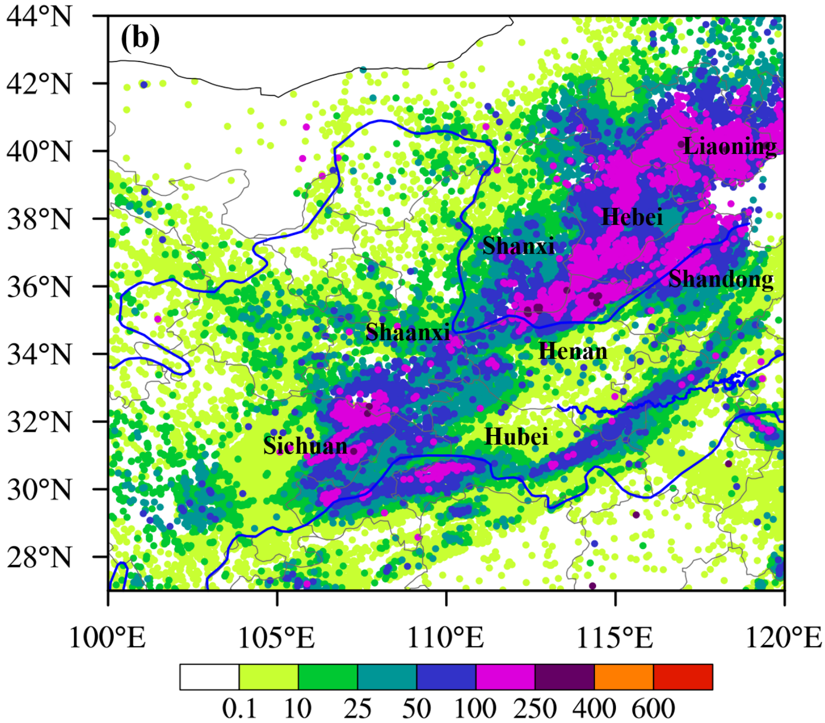

Figure 1. Panel (**a**) shows the track of the southwest vortex (red line with dots), where the grey shading is the terrain (m). Panel (**b**) illustrates the 3D-accumulated (from 10 July to 12 July 2021) precipitation at stations (shading dots; mm).

2. Data and Methods

2.1. Data

In this study, we used two types of data: (i) The ERA5 reanalysis data from European Centre for Medium-Range Weather Forecasts (ECMWF), which had a temporal resolution of hourly and a spatial resolution of $0.25° \times 0.25°$ [19]. This dataset was used for synoptic analyses, vorticity budget calculations, and backward trajectory analyses. (ii) The hourly precipitation observed by the stations from the China Meteorological Administration (CMA). This dataset was used to analyze the variation in the SWV-related rainfall.

2.2. Vorticity Budget

In order to describe the variation in a vortex, we used the relative vorticity (vorticity, hereinafter) averaged within the vortex's central region. This was because a surface integral of vorticity within a region equaled the velocity circulation along the boundary of the region (i.e., the Green's theorem). Therefore, the area-averaged vorticity budget was effective to show the vortex's evolutionary mechanisms. The vorticity budget equation used in this study had the following expression [11,20]:

$$\frac{\partial \zeta}{\partial t} = -\boldsymbol{V}_{\mathrm{h}} \cdot \nabla_{\mathrm{h}} \zeta - \omega \frac{\partial \zeta}{\partial p} + \boldsymbol{k} \cdot \left(\frac{\partial \boldsymbol{V}_{\mathrm{h}}}{\partial p} \times \nabla_{\mathrm{h}} \omega \right) - \beta v - (\zeta + f) \nabla_{\mathrm{h}} \cdot \boldsymbol{V}_{\mathrm{h}} + D(\zeta) \tag{1}$$

where t was the time, ζ was the vorticity, $\mathbf{V}_{\mathrm{h}}$ was the horizontal wind vector, ∇_{h} was the horizontal gradient operator, and ω was the vertical velocity in pressure coordinate. $\mathbf{k}$ was the unit vector in the zenith direction, v was the meridional wind, and $\beta = \frac{\partial f}{\partial y}$, where f was the Coriolis parameter [21]. As Equation (1) was developed in the pressure coordinate, for small-scale systems, calculation errors would be notable.

The term $\frac{\partial \zeta}{\partial t}$ was the local time derivative (LTD), which indicated the temporal variation in vorticity; term $-\mathbf{V}_{\mathrm{h}} \cdot \nabla_{\mathrm{h}} \zeta$ denoted the horizontal advection of vorticity (HAV); term $-\omega \frac{\partial \zeta}{\partial p}$ stood for the vertical advection of vorticity (VAV); term $\mathbf{k} \cdot \left(\frac{\partial \mathbf{V}_{\mathrm{h}}}{\partial p} \times \nabla_{\mathrm{h}} \omega \right)$ showed the tilting effects (TIL); term $-\beta v$ represented the advection of planet vorticity (APV); term $-(\zeta + f)\nabla_h \cdot \mathbf{V}_h$ was the stretching effect (STR); and term $D(\zeta)$ represented the residual effects (RES), mainly due to calculation errors, subgrid processes, and friction. In order to reflect the overall effect of the terms on the right-hand side of Equation (1) except for RES, we defined a total term as TOT = HAV + VAV + TIL + APV + STR. The ratio of LTD and TOT could represent the balance of the vorticity budget (1 meant completely balanced). In this study, the ratio of LTD/TOT had a mean value of around 0.81, implying that the budget equation was overall well balanced, although there were calculation errors.

2.3. Analysis Using Backward Trajectory

In order to investigate the formation mechanisms of the SWV, we employed the Hybrid Single Particle Lagrangian Integrated Trajectory Model (HYSPLIT) [22] to track the air particles that formed the SWV at the time when the vortex was generated [23]. The HYSPLIT model was developed by the National Oceanic and Atmospheric Administration (NOAA), which was a complete system for computing simple air parcel trajectories. It could also calculate the complex transport, dispersion, chemical transformation, and deposition associated with tracking air particles. According to the size of the SWV at its formation time, a total of 83 air particles (horizontal resolution is $0.25° \times 0.25°$) was determined to use in the backward tracking analyses. The backward trajectory analysis was initiated at 0200 UTC 10 July 2021, when the SWV was generated (Figure 1a), and ran for 24 h (ended at 0200 UTC 9 July 2021) to cover the whole formation stage of the SWV.

3. Overview of the Event

3.1. Precipitation Features

From 10 July to 12 July 2021, affected by lower-level shear lines and a SWV, a series of heavy rainfall appeared in Sichuan Province and Chongqing (Figure 1b), with the heavy rainfall centers mainly located in Bazhong City and Dazhou City. During the process, a total of 920 observational stations showed an accumulated precipitation of 50–99.9 mm; a total of 453 observational stations had an accumulated precipitation of 100–249.9 mm; and a total of 18 observational stations had an accumulated precipitation of above 250 mm. Observational stations with an accumulated precipitation of above 300 mm included Zhuyuan (327.2 mm) in Tongjiang County, Caomiaozi (327.6 mm) in Tongjiang County, and Chenjia (335.4 mm) in Dachuan County. The maximum daily rainfall was 304.7 mm, which occurred in Caomiaozi (Tongjiang County), and the maximum hourly rainfall was 99 mm, which appeared in Muzi (Dazhou City).

In addition to Sichuan and Chongqing, affected by the northeastward moving SWV (Figure 1b), Shaanxi, Henan, Shanxi, Hebei, Shandong, and Liaoning experienced heavy rainfall events successively from southwest to northeast (Figure 1b). The total precipitation band was mainly stretched in the southwest–northeast direction (corresponding to the SWV's track; Figure 1a). The heavy rainfall centers (accumulated precipitation $\geq$ 100 mm) mainly appeared in the junction regions of Henan, Shanxi, Hebei, and Shandong, the northern section of Shandong, and the northwestern sections of Hebei, Beijing, and Liaoning.

3.2. Synoptic Analyses

During the rainfall event, the South Asia High (SAH) dominated the Tibetan Plateau (Figure 2), with its closed center mainly located over the northern section of the Indian subcontinent. Strong upper-level jets mainly appeared in the regions north and northeast of the SAH (they were not directly related to the heavy rainfall in Sichuan), and they were broken into several sections. The Sichuan Basin was situated in the northeastern section of the SAH, where the upper-level divergence was strong. This was favorable for maintaining ascending motions (due to fluid continuity [21]) that acted as a crucial condition for heavy rainfall. Another striking feature for the upper troposphere was that there was a shortwave trough that moved eastward along the northern boundary of the SAH (Figure 2). Intense divergence appeared ahead of the trough, which favored appearance and maintenance of ascending motions around the Sichuan Basin. Moreover, this eastward-moving trough was closely related to the northeastward displacement of the SWV.

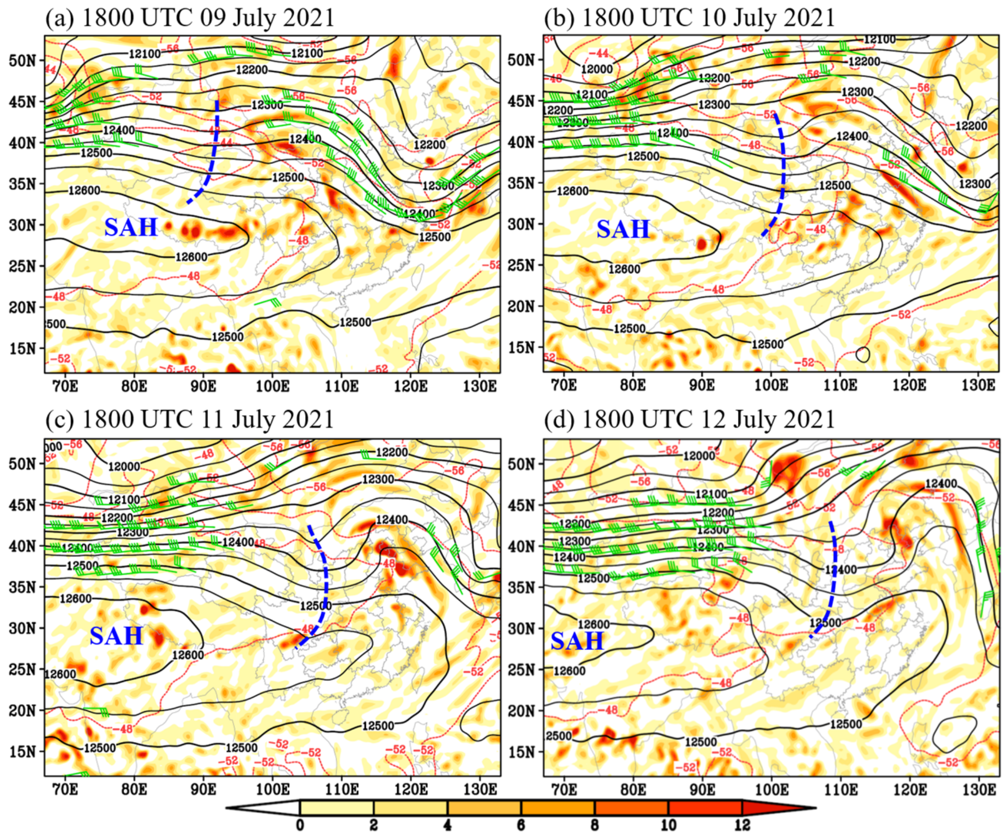

Figure 2. Panels (**a**–**d**) show the geopotential height (black contour; gpm), wind (green wind bar; a full bar represents 10 m s^{-1}), temperature (red contour; °C), and divergence at 200 hPa (shading; 10^{-5} s^{-1}), where the blue dashed lines show the trough lines, and SAH = South Asian High.

In the middle troposphere, the Western Pacific subtropical high (WPSH) was mainly located in the middle and low latitude regions (Figure 3). During the whole event, the WPSH sustained a strong intensity and kept its western boundary around 105° E or further west. Southerly and southwesterly winds along the WPSH's western boundary favored the northward transport of moisture for the heavy rainfall. Northwest of the WPSH, there was a shortwave trough (it corresponded to the 200 hPa shortwave trough), which moved eastward with time and enhanced in intensity gradually. Ahead of the trough, strong warm advection appeared (Figure 3), which contributed to promoting ascending motions through quasi-geostrophic forcings [21]. This favored the lowering of lower-level pressure [12], which acted as a favorable condition for the development/maintenance of the SWV. It should be noted that a mesoscale vortex (reflected by the closed center of the geopotential height) developed from 1800 UTC 9 July to 0600 UTC 12 July 2021 in the northern section of the shortwave trough. The vortex moved eastward with the shortwave trough and showed notable interactions with the SWVs.

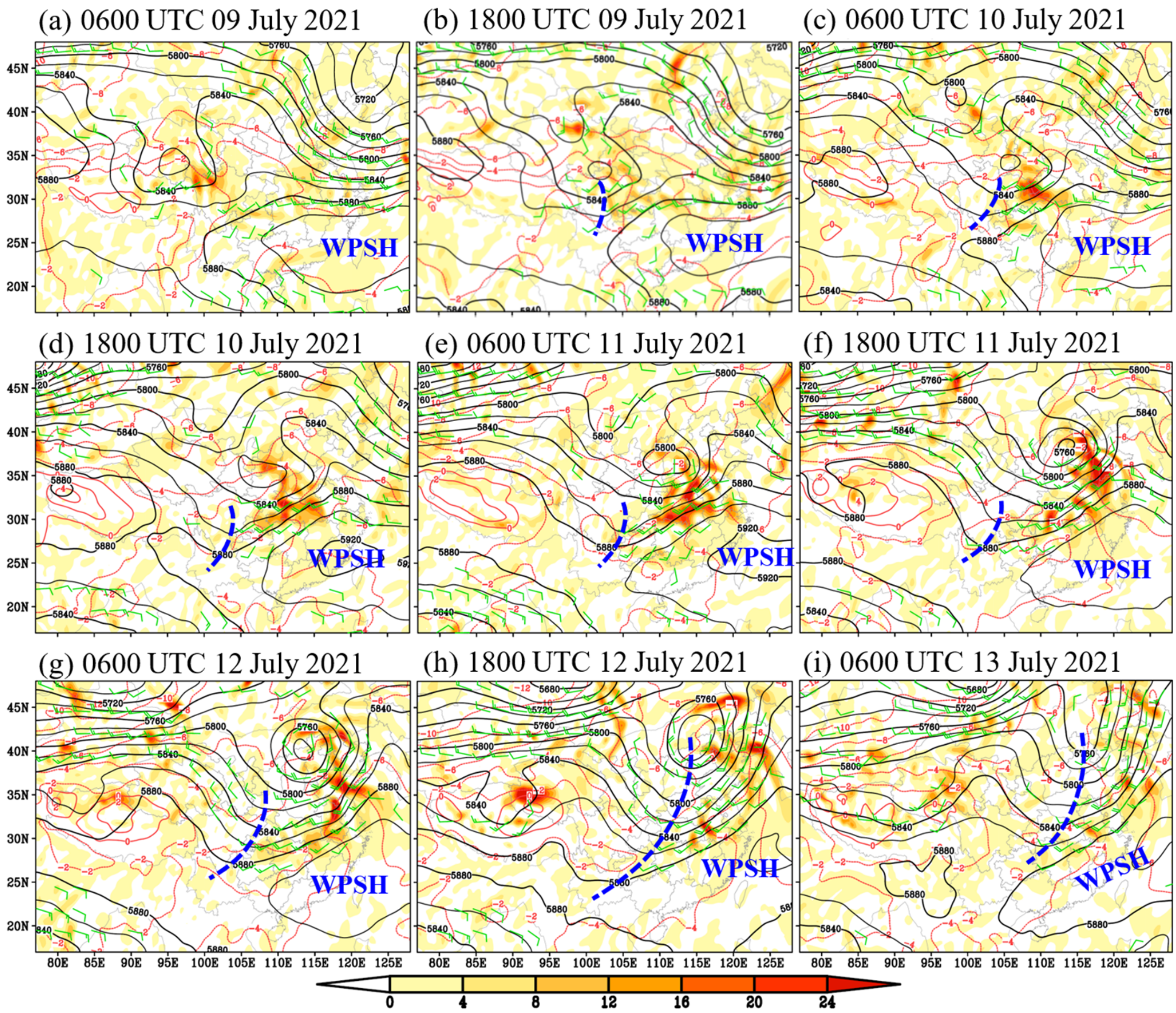

Figure 3. Panels (**a**–**i**) show the geopotential height (black contour; gpm), wind (green wind bar; a full bar represents 10 m s^{-1}), temperature (red contour; °C), and warm advection at 500 hPa (shading; 10^{-5} K s^{-1}), where the blue dashed lines show the trough lines, and WPSH = Western Pacific subtropical high.

In the lower troposphere, before the SWV's formation (i.e., 0200 UTC 10 July 2021), a high-pressure ridge dominated the regions east of the Tibetan Plateau (Figure 4a,b), west of which a shear line appeared in the western section of the Sichuan Basin (Figure 5a,b). In this stage, heavy rainfall was mainly produced by the lower-level shear line. After the SWV formed, a closed geopotential-height center appeared in the northern section of the Sichuan Basin (Figure 4c). The closed center was associated with a closed cyclonic circulation and a strong cyclonic vorticity (i.e., the SWV). A southwesterly low-level jet appeared in the southeastern section of the SWV and the regions east of the vortex (Figure 5c), which favored moisture transport for heavy rainfall, and, also, the jet contributed to maintain the convergence associated with the SWV [21]. From 1800 UTC 10 July to 0600 UTC 12 July 2021, the SWV moved northeastward and intensified with time. The intensification could be reflected by the strengthening of the closed geopotential-height center (Figure 4d–g), cyclonic-vorticity center, and low-level jet (Figure 5d–g). After that the SWV weakened in intensity (Figures 4g–i and 5g–i), and, finally, the SWV dissipated at 2000 UTC 12 July 2021. During this stage, the cyclonic vorticity and closed geopotential-height center both weakened with time (Figure 4g–i), whereas the meridional range of the low-level jet enlarged, which formed a broad moisture transport channel from lower-latitude regions to higher-latitude regions.

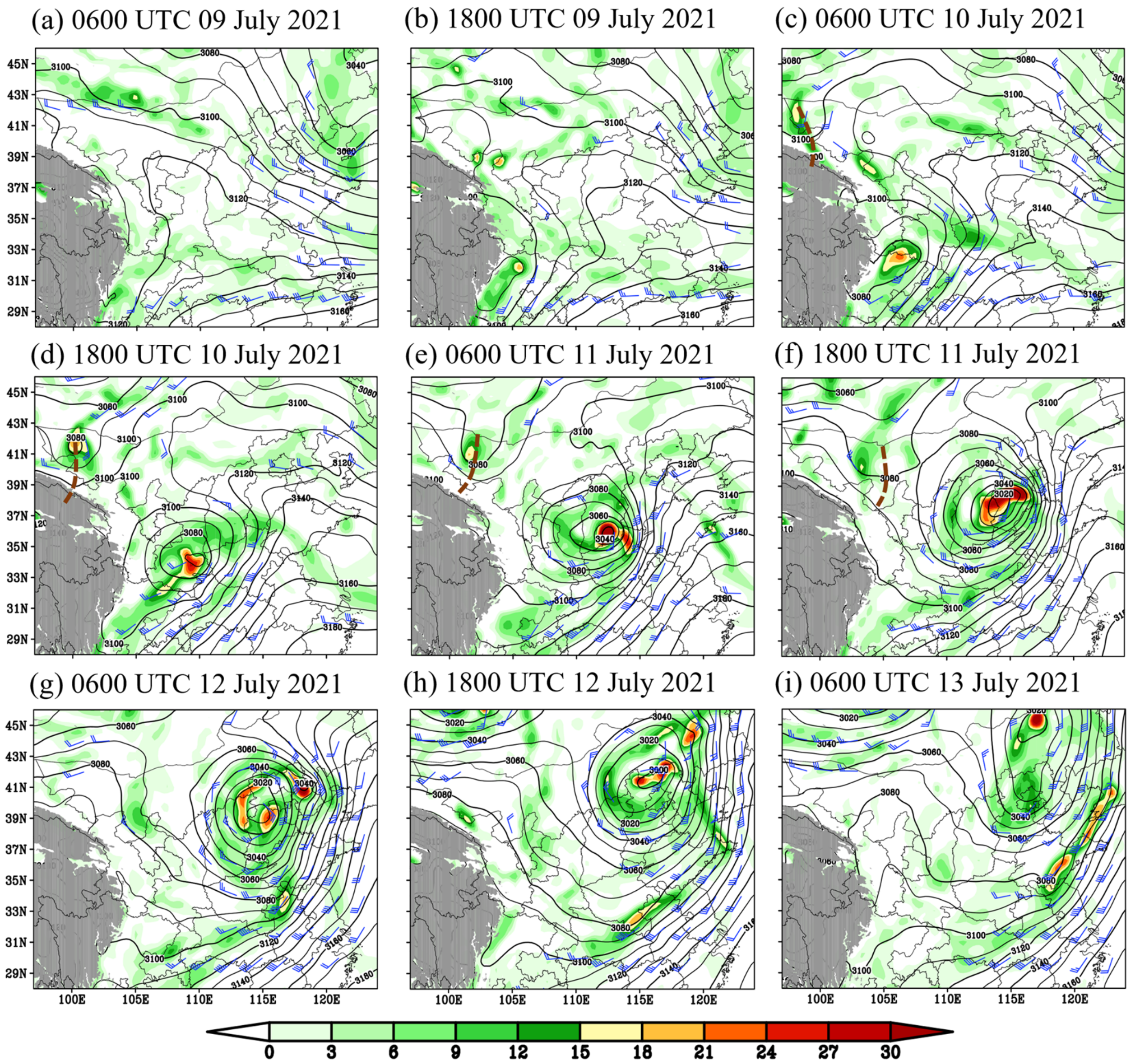

Figure 4. Panels (**a**–**i**) show the geopotential height (black contour; gpm), wind (blue wind bar; a full bar represents 4 m s^{-1}), and cyclonic vorticity at 700 hPa (shading; 10^{-5} s^{-1}), where the brown dashed lines are the trough lines, and the grey shading marks the terrain higher than 3000 m.

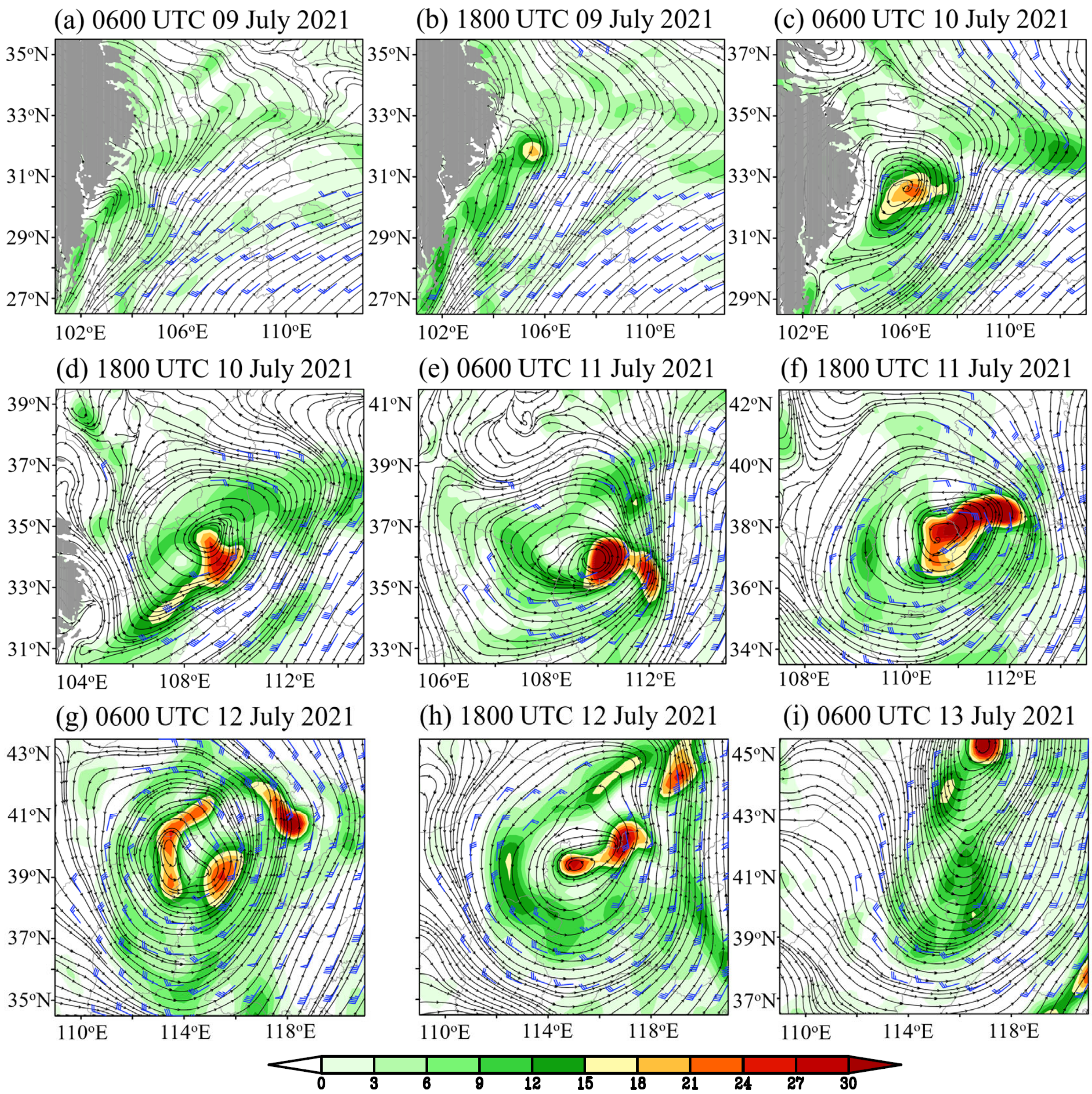

Figure 5. Stream field (black line with arrows), cyclonic vorticity (shading; 10^{-5} s^{-1}), and wind (blue wind bar; a full bar is 4 m s^{-1}) at 700 hPa, where the grey shading marks the terrain higher than 3000 m.

4. Evolution of the Southwest Vortex

4.1. Displacement of the Vortex

Before analyzing the SWV in detail, we first defined a central region for the vortex. The central region (i.e., a box of 2.5° × 2.5°) was determined by using the temporal mean size of the SWV during its whole life span. A sensitivity test was conducted to the central region, and it could be found that the central region-based analysis results were insensitive to relatively small changes (±0.25°) to each boundary of the box. As a result, the central region could be used as a representative for the SWV. As Figure 1a shows, the SWV formed around 0200 UTC 10 July 2021 in the northern section of the Sichuan Basin. After formation, the vortex first kept a quasi-stationary manner from 0200 UTC 10 to 1200 UTC 10 July 2021, and then it moved northeastward (from 1200 UTC 10 to 0300 UTC 11 July 2021), with the meridional moving speed smaller than the zonal moving speed. Following this, the meridional moving speed of the SWV increased (as the shortwave trough intensified notably, the northerly wind in its eastern section enhanced, which acted as the steering flow of the SWV; Figure 3g,h), which became larger than the zonal moving speed (from 2300 UTC 11 to 1400 UTC 12 July 2021). Finally, the SWV dissipated around 2000 UTC 12 July 2021 in the northern section of Hebei. Overall, the SWV lasted for a period of around 66 h.

4.2. Relation between the SWV and a Middle-Tropospheric Vortex

Similar to the SWVs investigated in previous studies [10], the SWV in this event was mainly located around 700 hPa, and thus we used the layer of 650–750 hPa to analyze its evolution. In addition to the SWV, a middle-tropospheric mesoscale vortex also appeared in this event and showed notable interactions with the SWV. From Figure 3b, it can be seen that the middle-tropospheric vortex (reflected by the closed geopotential-height contour of 5820 gpm) formed around 1800 UTC 09 July 2021 (~6 h earlier than the SWV's formation), within the central section of the shortwave trough. From 0600 UTC 10 to 0600 UTC 12 July 2021, the vortex intensified rapidly and moved northeastward with time (Figure 3c–g). Following this, the middle-tropospheric vortex weakened with time, and, finally, it dissipated around 0600 UTC 13 July 2021 (~10 h latter than the SWV's dissipation), over the junction region of Inner Mongolia and Hebei Province (Figure 3i). The middle-tropospheric vortex lasted for around 4 days, and its central layer was 450–550 hPa.

Around 3 h after the formation of the middle-level vortex at 700 hPa, a shortwave trough appeared below the vortex (Figure 4b). From 0600 UTC 10 to 1800 UTC 11 July 2021, the 700 hPa shortwave trough moved eastward along with the middle-level vortex and intensified with time (Figure 4c–f). Around 0000 UTC 12 July 2021, the 700 hPa shortwave trough merged into the closed cyclonic circulation of the SWV (Figure 4g), which corresponded to the vertical coupling of the middle-level mesoscale vortex with the SWV (Figures 3g and 4g). After the coupling, both the middle-level vortex and the SWV enhanced notably, which could be reflected by the central region-averaged cyclonic vorticity at the layer of 750–450 hPa (Figure 6a). From 0000 UTC 12 July 2021, under the steering of the strong southerly wind within the eastern section of the shortwave trough, the coupling vortex moved northward rapidly (Figure 3g–i) and caused heavy precipitation in Hebei and Liaoning (Figure 1b). Overall, the correlation between the central region-averaged vorticity of the SWV and that of the middle-level vortex was around 0.91, implying that the two vortices showed consistent evolutionary features to each other.

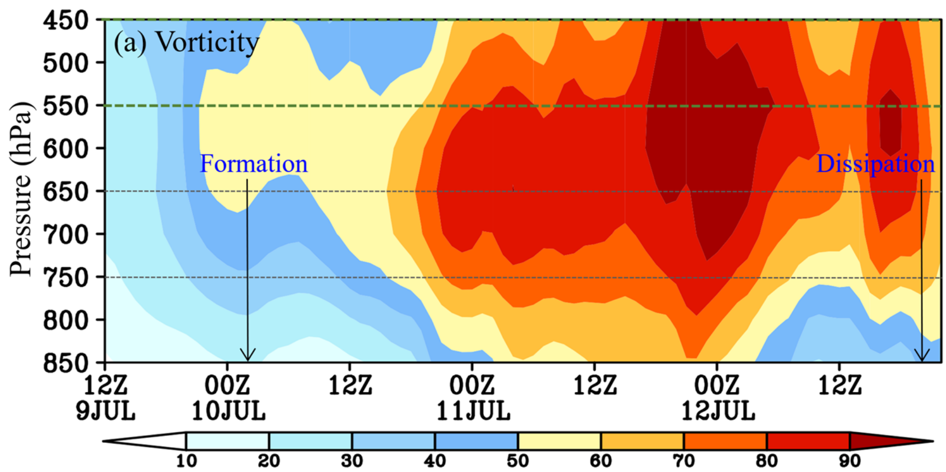

Figure 6. *Cont.*

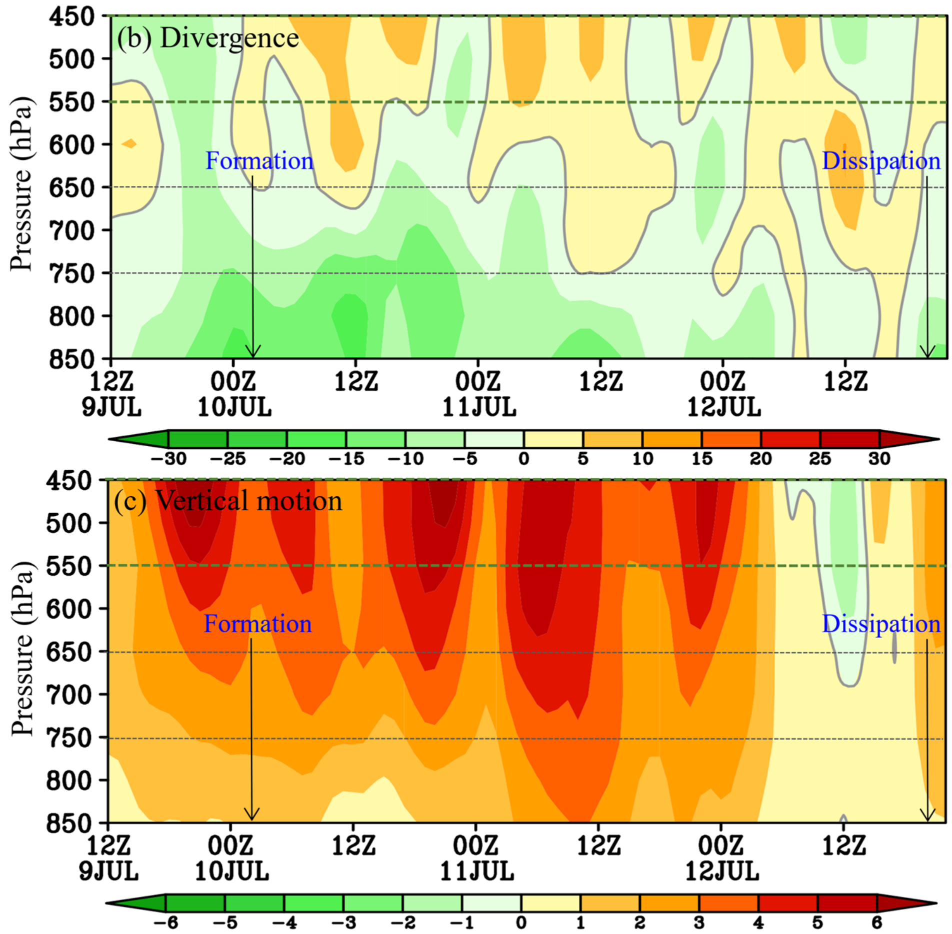

Figure 6. Panel (**a**) shows the central region-averaged vorticity (shading; 10^{-6} s^{-1}), where the grey dashed lines outline the central layer of the southwest vortex, the green dashed lines outline the central layer of the middle-level vortex, and the two arrows show the formation and dissipation time of the southwest vortex. Panel (**b**) is the same as (**a**) but for the divergence (shading; 10^{-6} s^{-1}), where the thick grey contour is the zero isoline of divergence. Panel (**c**) is the same as (**a**) but for the vertical motion (shading; cm s^{-1}), where the thick grey contours are the zero isolines of vertical velocity.

4.3. Evolutionary Feature of the Southwest Vortex

In this study, the central region-averaged values (i.e., a box of 2.5° × 2.5° centered at the SWV's center) were used to represent the overall features of the SWV. As Figure 6a shows, in the layer of 750–650 hPa (i.e., the central level of the SWV), cyclonic vorticity was strong, which corresponded to the SWV. According to the vertical mean (from 750 hPa to 650 hPa) of the central region-averaged vorticity (VMCV), the evolution of the SWV could be divided into four stages: (i) the formation stage (from 1200 UTC 09 to 0100 UTC 10, July 2021), during which the VMCV increased rapidly from 2.1×10^{-5} s^{-1} to 4.8×10^{-5} s^{-1}; (ii) the developing stage (from 0200 UTC 10 to 0000 UTC 11, July 2021), during which the VMCV increased quickly from 4.7×10^{-5} s^{-1} to 8.3×10^{-5} s^{-1}; (iii) the maintaining stage (from 0100 UTC 11 to 0000 UTC 12, July 2021), during which the VMCV increased slowly from 8.1×10^{-5} s^{-1} to 9.3×10^{-5} s^{-1}; and (iv) the decaying stage (from 0100 UTC 12 to 2000 UTC 12, July 2021), during which the VMCV decreased rapidly from 9.2×10^{-5} s^{-1} to 6.1×10^{-5} s^{-1}.

During the formation stage (from 1200 UTC 09 to 0100 UTC 10, July 2021), mainly due to the enhancement of the low-level jet (Figure 4a,b), the convergence within the SWV's central region enhanced (Figure 6b), and, as a result, the ascending motions also intensified (Figure 6c). Meanwhile, the central region-averaged zonal wind increased (Figure 7a), meridional wind first increased and then decreased (Figure 7b), and, as the cold pool (due to evaporative cooling of precipitation) was still weak, the central region-averaged temperature changed slowly (Figure 7c). During the developing stage (from 0200 UTC 10 to 0000 UTC 11, July 2021), corresponding to the enhancement of the low-level jet (Figure 4c,d), the central region-averaged convergence became stronger (Figure 6b). Meanwhile, the ascending motions kept a strong intensity with two peaks appearing in this stage (Figure 6c). The central region-averaged zonal and meridional winds were strong (Figure 7a,b), implying the SWV showed a high potential to move. The central region-averaged temperature decreased notably, which corresponded to the enhanced evaporative cooling of precipitation. During the maintaining stage (from 0100 UTC 11 to 0000 UTC 12, July 2021), convergence within the central region decreased (Figure 6b), with divergence appearing in some periods. The central region-averaged ascending motions reached the maximum intensity in this stage (Figure 6c), corresponding to the heavy rainfall (not shown). The central region-averaged zonal and meridional winds mainly decreased (Figure 7a,b), and the central region-averaged temperature also decreased notably (Figure 7c; due to the intensifying of evaporative cooling of precipitation). During the decaying stage (from 0100 UTC 12 to 2000 UTC 12, July 2021), within the central region of the SWV, the divergence increased notably and dominated the central region (Figure 6b), ascending motions decreased significantly (Figure 6c), the zonal wind increased (Figure 7a), the meridional wind decreased (Figure 7b), and the temperature changed slowly (Figure 7c). Overall, in this stage, the conditions became no longer favorable for the SWV's sustainment, and thus the vortex dissipated.

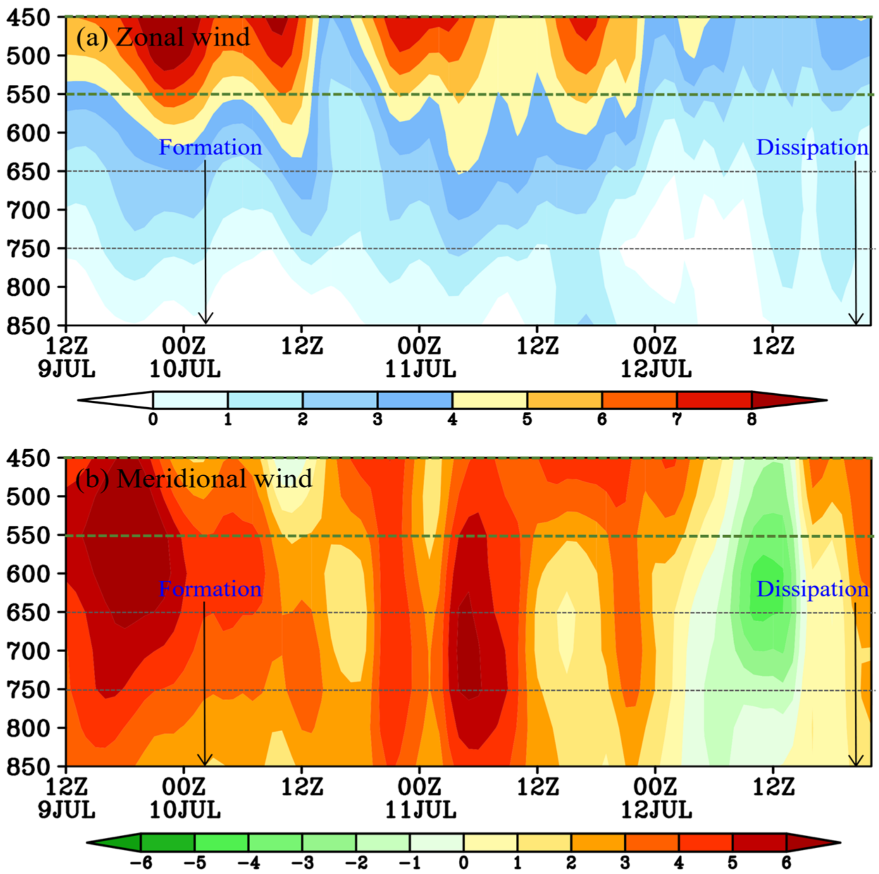

Figure 7. *Cont.*

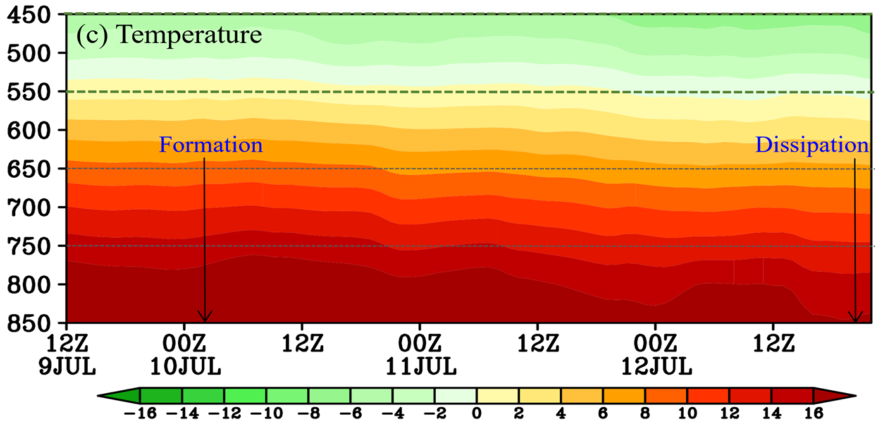

Figure 7. Panel (**a**) shows the central region-averaged zonal wind (shading; m s^{-1}), where the grey dashed lines outline the central layer of the southwest vortex, the green dashed lines outline the central layer of the middle-level vortex, and the two arrows show the formation and dissipation time of the southwest vortex. Panel (**b**) is the same as (**a**) but for the meridional wind (shading; m s^{-1}). Panel (**c**) is the same as (**a**) but for the temperature (shading; °C).

5. Mechanisms Governing the Evolution of the Southwest Vortex

5.1. Vorticity Budget

In this study, the vorticity budget results by using Equation (1) were averaged within the central region of the SWV to show the mechanisms governing the evolution of the vortex. This method was widely used in previous studies [10–12,23]. As Figure 8a shows, term TOT was strongly positive (750–650 hPa) during the formation stage (from 1200 UTC 09 to 0100 UTC 10, July 2021) and developing stage (from 0200 UTC 10 to 0000 UTC 11, July 2021) of the SWV. This corresponded to the formation and rapid development of the SWV. The convergence-related vertical stretching (i.e., STR) acted as the most favorable factor for the SWV's formation and development (Figure 8d). The upward transport of cyclonic vorticity by ascending motions (i.e., VAV) was the second dominant factor (Figure 8c). The tilting effects (i.e., TIL) were the most detrimental factor (Figure 8e). The horizontal transport caused a net export of cyclonic vorticity from the SWV's central region (Figure 8b), which slowed down the cyclonic vorticity's increase. During the maintaining stage (from 0100 UTC 11 to 0000 UTC 12, July 2021), the vertical transport of vorticity enhanced notably (Figure 8c) since ascending motions within the central region of SWV became stronger (Figure 6c). As a result, the VAV became the most favorable factor for the SWV's maintenance. In this stage, the convergence-related vertical stretching decreased notably (Figure 8d) because the central region-averaged convergence became weaker (Figure 6b). However, the overall effects of STR during the maintaining stage were still positive. Tilting effects enhanced in intensity, which acted as the most detrimental factor for the increase in cyclonic vorticity (Figure 8e). Net import/export transport of cyclonic vorticity into the central region of SWV appeared in the latter/earlier period of the maintaining stage (Figure 8b), and the overall effect of HAV was still negative. During the decaying stage, cyclonic vorticity within the SWV's central region decreased mainly due to the net export transport of cyclonic vorticity (Figure 8b) and the tilting effects (Figure 8e). In addition, as the divergence became dominant within the SWV's central region during this stage (Figure 6b), STR showed an overall negative effect for the SWV's maintaining (Figure 8d). In contrast, the vertical transport of vorticity served as the most important factor that resisted the SWV's weakening (Figure 8c). In summary, the factors that dominated different stages of the SWV's evolution were shown in Table 1.

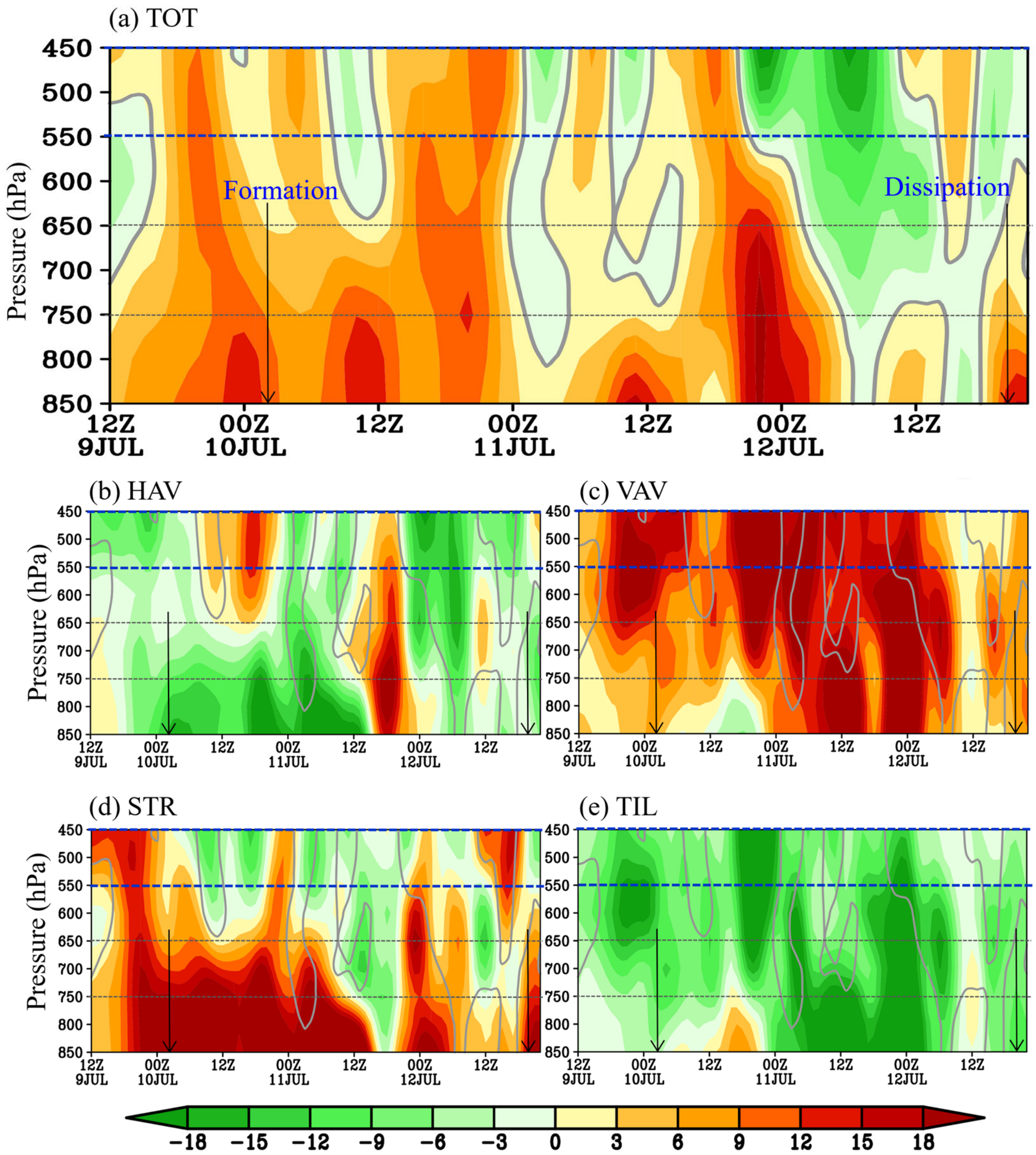

Figure 8. Panel (**a**) shows the central region-averaged term TOT (shading; 10^{-10} s^{-2}), where the thick grey contour is the zero isoline of TOT, the grey dashed lines outline the central layer of the southwest vortex, the blue dashed lines outline the central layer of the extratropical cyclone, and the two arrows show the formation and dissipation time of the southwest vortex. Panel (**b**) is the same as (**a**) but for term HAV (shading; 10^{-10} s^{-2}). Panel (**c**) is the same as (**a**) but for term VAV (shading; 10^{-10} s^{-2}). Panel (**d**) is the same as (**a**) but for term STR (shading; 10^{-10} s^{-2}). Panel (**e**) is the same as (**a**) but for term TIL (shading; 10^{-10} s^{-2}).

Table 1. Factors dominated different stages of the SWV's evolution. HAV = horizontal advection of vorticity; VAV = vertical advection of vorticity; TIL = tilting effects; STR = stretching effect. "/" means none.

	Formation Stage	Developing Stage	Maintaining Stage	Decaying Stage
Most favorable factors	STR	STR	VAV	VAV
Other favorable factors	VAV	VAV	STR	/
Most detrimental factors	TIL	TIL	TIL	TIL, HAV
Other detrimental factors	HAV	HAV	HAV	STR

5.2. Backward Trajectory Analyses

In order to understand the formation of the SWV, we used the backward trajectory analyses to investigate the changes in the air particles (that formed the SWV at the time when it formed). At the time when the SWV formed, a closed cyclonic circulation that was coupled with a closed geopotential-height center (i.e., 3078 gpm) appeared in the northern section of the Sichuan Basin (Figure 9a). A total of 83 points (at an interval of 0.25°) within the closed geopotential-height contour of 3078 gpm (Figure 9b) was selected to stand for the SWV's main body. These air particles were used in the backward tracking. The backward tracking was initiated at 0200 UTC 10 July 2021 and ran for 24 h to cover the whole formation stage of the SWV. The tracks of the 83 air particles were shown in Figure 9c. It was shown that ~68.7% of the air particles came from the height below 2500 m, ~21.7% came from the height around 3000 m (i.e., 2500–3500 m), and only ~9.6% came from the height higher than 3500 m. This meant that the air particles sourced from the lower troposphere were crucial for the SWV's formation. Compared the initial height (at 0200 UTC 09 July 2021) with the final height (at 0200 UTC 10 July 2021), ~94.0% of the 83 air particles experienced ascending (i.e., the final height was higher than the initial height) during the formation stage of the SWV. Of all the air particles that formed the SWV, around 6.0% of them passed through the Hengduan Mountain (southwest of the Sichuan Basin), ~48.2% passed through the Yunnan–Guizhou Plateau (south of the Sichuan Basin), and ~45.8% of them came from the Sichuan Basin.

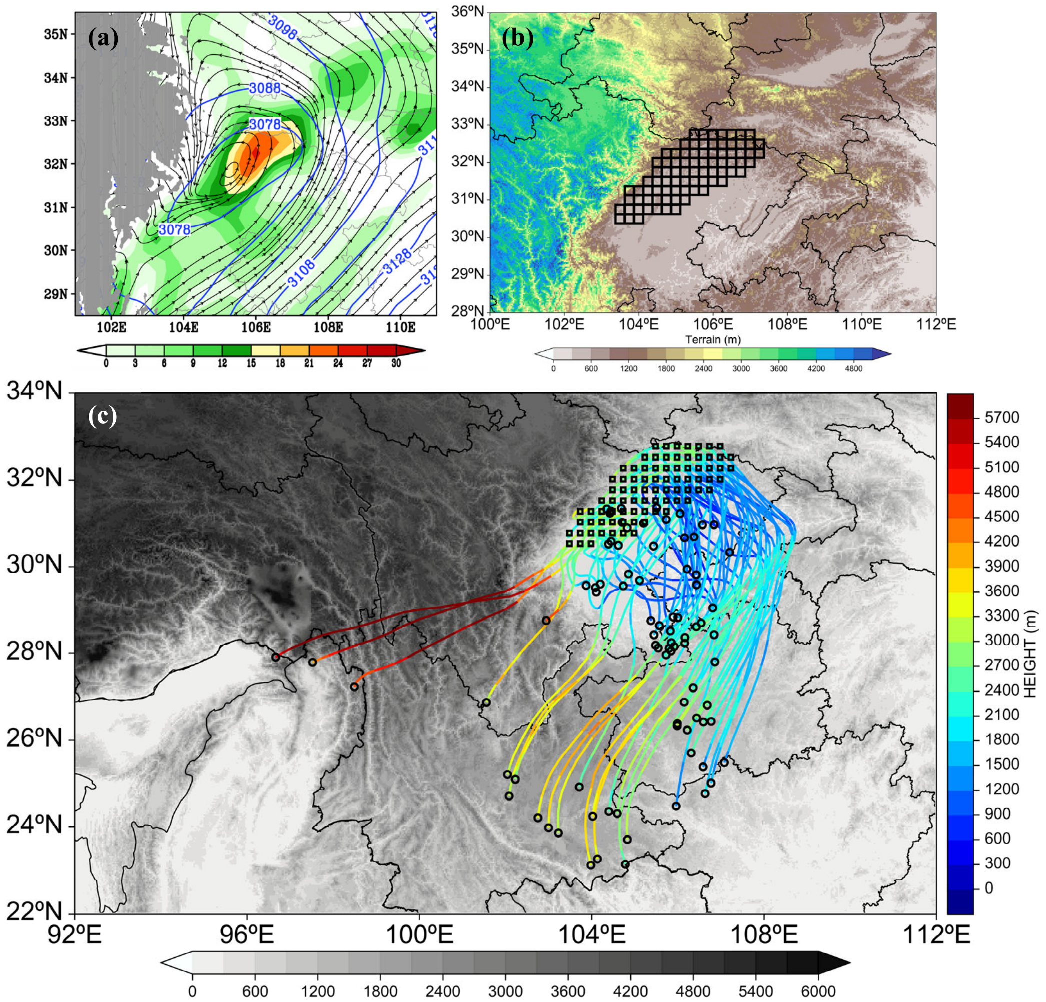

Figure 9. Panel (**a**) shows the geopotential height (blue contour; gpm), stream field (black lines with arrows), and cyclonic vorticity (shading; 10^{-5} s^{-1}) at 700 hPa, where the grey shading marks the

terrain higher than 3000 m. Panel (**b**) shows the locations of the air particles used for backward tracking (black boxes), where shading is terrain. Panel (**c**) shows the trajectories of the air particles (shading tracks), where small black circles mark the locations of the air particles 24 h before the formation of the southwest vortex, and the small black boxes mark the locations when the southwest vortex formed.

When the SWV formed, ~98.8% of the air particles that formed the vortex had a cyclonic vorticity (Figure 10a; overall, the SWV had a mean vorticity of 1.4×10^{-4} s^{-1} within the closed geopotential-height contour of 3078 gpm), whereas only ~59% of the air particles showed a convergence feature (Figure 10b; overall, the SWV had a mean divergence of -2.3×10^{-5} s^{-1}). Comparing the final state (at 0200 UTC 10 July 2021) with the initial state (at 0200 UTC 09 July 2021), ~96.4% of the air particles experienced an increase in cyclonic vorticity (Figure 10c). In contrast, the proportion of the air particles that experienced an increase in convergence was ~53.0% (Figure 10d). Comparisons among the air particles that passed through the Hengduan Mountain, the Yunnan–Guizhou Plateau, and the Sichuan Basin showed that the second type showed the strongest increases in overall convergence and cyclonic vorticity (Figure 10a,b). In contrast, the first type showed the weakest intensity of convergence and cyclonic vorticity. This meant that the air particles that passed through the Yunnan–Guizhou Plateau played a crucial role in the SWV's formation. These air particles descended along the topography of the Yunnan–Guizhou Plateau, during which their cyclonic vorticity and convergence mainly intensified (Figure 10a,b). This indicated that the topography of the Yunnan–Guizhou Plateau showed an important impact on the SWV's formation. Those air particles that passed through the Hengduan Mountain also enhanced notably in their cyclonic vorticity when they descended from the Hengduan Mountain (Figure 10a), whereas they mainly showed a divergence feature (Figure 10b). Mechanisms governing the variations in the air particles' vorticities and divergences were complicated, which required further study in the future.

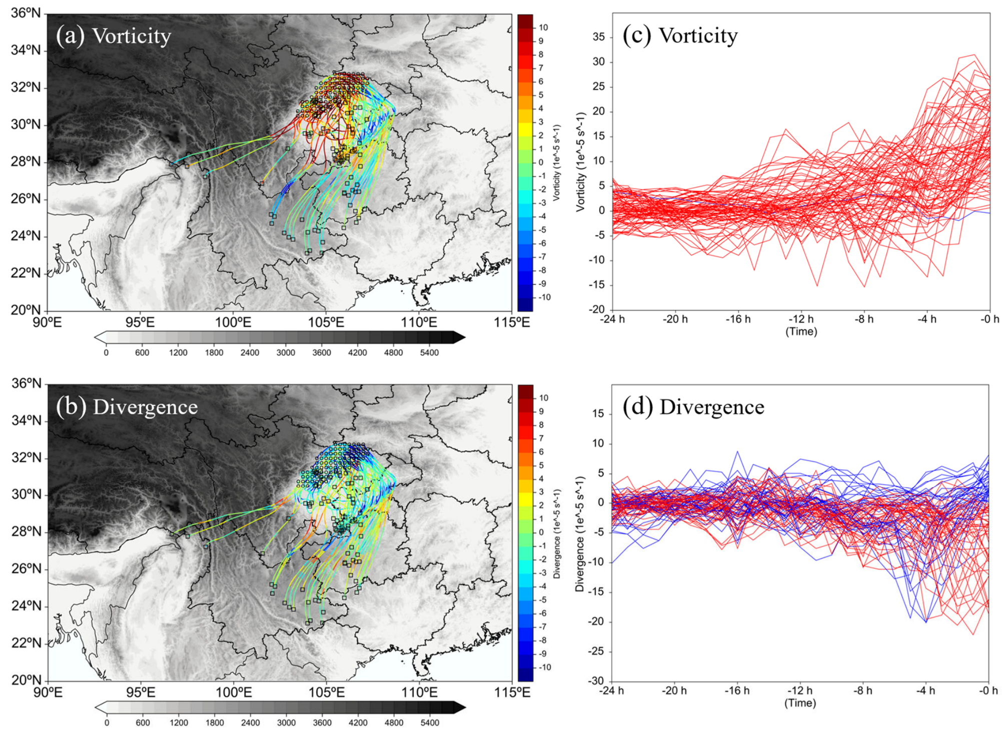

Figure 10. Panel (**a**) shows the vorticity along the trajectories (shading; 10^{-5} s^{-1}), where the small black boxes mark the locations of the air particles at the time 24 h before the southwest vortex's formation, the small black circles mark the locations of the air particles at the time when the vortex

formed, and the grey shading is terrain (m). Panel (**b**) is the same as (**a**) but for the divergence (shading; 10^{-5} s^{-1}). Panel (**c**) shows the variation in vorticity (10^{-5} s^{-1}) from the time 24 h before the southwest vortex's formation to the time when the vortex formed, where red lines show the air particles that had cyclonic vorticity when the SWV formed, and the blue lines show the air particles that had anti-cyclonic vorticity. Panel (**d**) is the same as (**c**) but for the divergence (10^{-5} s^{-1}), where the red lines show the air particles that had convergence when the SWV formed, and the blue lines show the air particles that had divergence.

6. Conclusions and Discussion

During the period from 10 July to 12 July 2021, regions in Southwest, Central, North, and Northeast China experienced a series of heavy rainfall events successively. This resulted in severe economic losses. One of the most striking features for this event was that a long-lived (~66 h) northeastward-moving SWV served as a dominant weather system that induced the heavy precipitation. The SWV deserved a detailed study, as its lifespan (~66 h) was much longer than the SWVs' mean lifespan, and the SWV moved for a distance of ~2000 km, whereas the vast majority of SWVs showed a quasi-stationary behavior [10,24,25].

It was found that the SWV formed and sustained in favorable background environments, which were characterized by a strong SAH-related upper-level divergence, a notable middle-tropospheric shortwave trough related warm advection, and a vigorous low-level jet. A deep shortwave trough (stretched from 200 hPa to 500 hPa) east of the Tibetan Plateau was crucial for the SWV's displacement, as the strong southwesterly wind in the eastern section of the trough acted as the steering flow for the vortex. Another favorable condition for the SWV's displacement were the interactions between the SWV and a middle-tropospheric mesoscale vortex: the vertical coupling of the two vortices enhanced, and they both moved northeastward under the southwesterly steering flow. According to the VMCV, a total of four stages were defined for the SWV: the formation stage, the developing stage, the maintaining stage, and the decaying stage. Overall, during different stages, the SWV showed notably different features in terms of vorticity, divergence, three-dimensional winds, and temperature. The vorticity budget showed that the convergence-related vertical stretching (i.e., STR) acted as the dominant factor for the SWV's formation and development; the upward transport of cyclonic vorticity (i.e., VAV) by ascending motions was the most favorable factor for the SWV's sustainment, whereas, during the decaying stage, the SWV dissipated mainly due to the tilting effects (i.e., TIL) and the net export transport of cyclonic vorticity from the SWV's central region (i.e., HAV). Backward trajectory analyses show that the air particles sourced from lower troposphere were crucial for the SWV's formation, and, during the formation stage, most of the air particles experienced notable ascending motions. Around 96.4% of the air particles that formed the SWV when it formed experienced an increase in cyclonic vorticity (Figure 10c), whereas the proportion of the air particles that experienced an increase in convergence was ~53.0%. The topography of the Yunnan–Guizhou Plateau showed an important impact on the SWV's formation, as ~48.2% of the air particles that formed the SWV came from this region, and most of these air particles enhanced in their cyclonic vorticity and convergence when they descended along the topography of the Yunnan–Guizhou Plateau.

As discussed above, this study showed some interesting results on a rarely seen type of SWV (i.e., long-lived and northeastward moving), which provided a supplement to the existing studies of SWVs. However, for a case study, its representativeness had significant limitations. Moreover, in this study, we mainly analyzed the SWV by using the ERA5 reanalysis data, which could not show the fine three-dimensional structures of the SWV. Therefore, we intend to investigate more SWV cases by using high-resolution numerical simulations in the future. This would be useful to reach a more comprehensive understanding of the SWVs.

Author Contributions: Conceptualization, K.-Q.Y., X.-W.J. and S.-M.F.; methodology, K.-Q.Y. and D.-X.X.; data collection and analysis, K.-Q.Y., D.-X.X., X.-W.J. and Z.-R.L.; writing—original draft, K.-Q.Y. and D.-X.X.; writing—review and editing, K.-Q.Y., X.-W.J., Z.-R.L. and S.-M.F. All authors have read and agreed to the published version of the manuscript.

Funding: This research was supported by the Sichuan Science and Technology Program (2022YFS0542, 2022YFS0540); National Natural Science Foundation of China (U20A2097, 42075002); the Innovation Team Fund of Southwest Regional Meteorological Center, China Meteorological Administration (XNQYCXTD-202202); and the Open Grants of the State Key Laboratory of Severe Weather (2021LASW-A06).

Institutional Review Board Statement: Not applicable.

Informed Consent Statement: Not applicable.

Data Availability Statement: The data used in this research are available upon request.

Acknowledgments: This research was supported by the Sichuan Science and Technology Program (2022YFS0542, 2022YFS0540); National Natural Science Foundation of China (U20A2097, 42075002); the Innovation Team Fund of Southwest Regional Meteorological Center, China Meteorological Administration (XNQYCXTD-202202); and the Open Grants of the State Key Laboratory of Severe Weather (2021LASW-A06).

Conflicts of Interest: The authors declare no conflict of interest.

References

1. Evans, C.; Weisman, M.L.; Bosart, L.F. Development of an intense, warm-core mesoscale vortex associated with the 8 May 2009 "Super Derecho" convective event. *J. Atmos. Sci.* **2014**, *71*, 1218–1240. [CrossRef]
2. Li, W.; Xia, R.; Zhong, Q.; Wang, Y. Vorticity and moisture budget analyses on a plateau vortex that cause an intense rainfall event within the Qaidam Basin. *Atmos. Sci. Lett.* **2021**, *22*, e1040. [CrossRef]
3. Fu, S.-M.; Zhang, J.-P.; Tang, H.; Jiang, L.-Z.; Sun, J.-H. A new mesoscale-vortex identification metric: Restricted vorticity and its application. *Environ. Res. Lett.* **2020**, *15*, 124053. [CrossRef]
4. Lu, J.-H. *Generality of the Southwest Vortex*; China Meteorological Press: Beijing, China, 1986.
5. Cheng, X.; Li, Y.; Xu, L. An analysis of an extreme rainstorm caused by the interaction of the Tibetan Plateau vortex and the Southwest China vortex from an intensive observation. *Meteorol. Atmos. Phys.* **2015**, *128*, 373–399. [CrossRef]
6. Chen, Z.-M.; Min, W.-B. Statistics analysis of southwest vortices. In *The Secondary Proceedings of Qingzang Plateau Meteorology Conference*; China Meteorological Press: Beijing, China, 2000; pp. 368–378.
7. Chen, Z.-M.; Xu, M.-L.; Min, W.-B.; Miu, Q. Relationship between abnormal activities of southwest vortex and heavy rain the upper reach of Yangtze River during summer of 1998. *Plateau Meteorol.* **2003**, *22*, 162–167.
8. Chen, Y.; Li, Y.; Qi, D. Analysis of the convective characteristics during the mutual evolution of an inverted trough/low vortex and its induced rainstorm over the northeastern Sichuan basin, China. *Meteorol. Atmos. Phys.* **2018**, *131*, 807–825. [CrossRef]
9. Feng, X.; Liu, C.; Fan, G.; Liu, X.; Feng, C. Climatology and Structures of Southwest Vortices in the NCEP Climate Forecast System Reanalysis. *J. Clim.* **2016**, *29*, 7675–7701. [CrossRef]
10. Fu, S.; Li, W.; Sun, J.; Zhang, J.; Zhang, Y. Universal evolution mechanisms and energy conversion characteristics of long-lived mesoscale vortices over the Sichuan Basin. *Atmos. Sci. Lett.* **2015**, *16*, 127–134. [CrossRef]
11. Fu, S.-M.; Sun, J.-H.; Luo, Y.-L.; Zhang, Y.-C. Formation of Long-Lived Summertime Mesoscale Vortices over Central East China:Semi-Idealized Simulations Based on a 14-Year Vortex Statistic. *J. Atmos. Sci.* **2017**, *74*, 3955–3979. [CrossRef]
12. Yang, R.; Zhang, Y.; Sun, J.; Li, J. The comparison of statistical features and synoptic circulations between the eastward-propagating and quasi-stationary MCSs during the warm season around the second-step terrain along the middle reaches of the Yangtze River. *Sci. China Earth Sci.* **2020**, *63*, 1209–1222. [CrossRef]
13. Wu, G.; Ma, T.; Liu, Y.; Jiang, Z. PV-Q Perspective of Cyclogenesis and Vertical Velocity Development Downstream of the Tibetan Plateau. *J. Geophys. Res. Atmos.* **2020**, *125*, e2019JD030912. [CrossRef]
14. He, G.-B. Review of southwest vortices research. *Meteorol. Mon.* **2012**, *38*, 155–163.
15. Zhou, Y.-S.; Yan, L.; Wu, T.-Y.; Xie, Z.-M. Comparative analysis of two rainstorm processes in Sichuan Province affected by the Tibetan Plateau vortex and southwest vortex. *Chin. J. Atmos. Sci.* **2019**, *43*, 813–830.
16. Luo, S.-W. *Research on Several Types of Weather Systems over the Qinghai Xizang Plateau and Its Neighboring Regions*; China Meteorological Press: Beijing, China, 1992; 205p.
17. Wang, Q.-W.; Tan, Z.-M. Multi-scale topographic control of southwest vortex formation in Tibetan Plateau region in an idealized simulation. *J. Geophys. Res. Atmos.* **2014**, *119*, 11543–11561. [CrossRef]
18. Ni, C.; Li, G.; Xiong, X. Analysis of a vortex precipitation event over Southwest China using AIRS and in situ measurements. *Adv. Atmos. Sci.* **2017**, *34*, 559–570. [CrossRef]

19. Hersbach, H.; Bell, B.; Berrisford, P.; Hirahara, S.; Horányi, A.; Muñoz-Sabater, J.; Nicolas, J.; Peubey, C.; Radu, R.; Schepers, D.; et al. The ERA5 global reanalysis. *Q. J. R. Meteorol. Soc.* **2020**, *146*, 1999–2049. [CrossRef]
20. Kirk, J.R. Comparing the Dynamical Development of Two Mesoscale Convective Vortices. *Mon. Weather Rev.* **2003**, *131*, 862–890. [CrossRef]
21. Holton, J.R. *An Introduction to Dynamic Meteorology*; Academic Press: San Diego, CA, USA, 2004; 552p.
22. Stein, A.F.; Draxler, R.R.; Rolph, G.D.; Stunder, B.J.B.; Cohen, M.D.; Ngan, F. NOAA's HYSPLIT Atmospheric Transport and Dispersion Modeling System. *Bull. Am. Meteorol. Soc.* **2015**, *96*, 2059–2077. [CrossRef]
23. Chen, Y.; Li, Y. Analysis of a Late-Autumn Rainstorm in the Sichuan Basin on the Eastern Side of the Tibetan Plateau. *Adv. Meteorol.* **2019**, *2019*, 1–21. [CrossRef]
24. Li, Y.-Q. New related progress on researches of the vortex source of southwest China vortex. *Plateau Meteorol.* **2021**, *40*, 1394–1406.
25. Lu, P.; Li, Y.-Q. Simulation of effect of subtropical high enhancement on southwest vortex. *Chin. J. Atmos. Sci.* **2021**, *45*, 851–862.